Nano Energy 131 (2024) 110305

Contents lists available at ScienceDirect

Nano Energy

journal homepage: www.elsevier.com/locate/nanoen

Multiphase soft metal enabled high-performance fabric-based wearable energy harvesting☆

Jiangtao Guo [a], Liangfei Duan [a,*], Wen Yang [a], Qin Wang [a], Yunbo Zhang [a], Yong Zhang [b], Zhong Lin Wang [c], Peizhi Yang [a,*]

[a] Key Laboratory of Renewable Energy Advanced Materials and Manufacturing Technology, Ministry of Education, Faculty of Chemistry and Chemical Engineering, Yunnan Normal University, Kunming 650500, China
[b] Department of Electrical and Computer Engineering, The University of North Carolina at Charlotte, Charlotte, NC 28223, USA
[c] Beijing Institute of Nanoenergy and Nanoscience, Chinese Academy of Sciences Beijing, China

ARTICLE INFO

Keywords:
Liquid metals
Multiphase soft metals
Wearable electronics
Flexible triboelectric nanogenerator
Energy harvesting
Self-powered system

ABSTRACT

Highly efficient and flexible power sources have always been the focus and goal in the field of wearable electronics. However, the existing wearable power sources are limited by their large size, high weight, electrolyte leakage, and poor mechanical compliance, which seriously hinders their practical applications. Herein, we propose a novel strategy to achieve and demonstrate a fabric-based high-performance wearable triboelectric nanogenerator (TENG) structure. The metals of gallium (Ga), bismuth (Bi), indium (In), and tin (Sn) are mixed according to specific mass ratios, and then they are transformed in liquid phase to form room-temperature multiphase soft metals of GaBiInSn. The material exhibits both metallic and fluidic properties, and possesses a characteristic of multiphase structure. The GaBiInSn material is directly deposited between polytetrafluoroethylene (PTFE) layers and nonwoven fabrics to establish multi-level conductive and frictional interfaces, creating charge transfer and solid-liquid hybrid dielectric layers. Therefore, the thin film-type triboelectric nanogenerators with a structure of PTFE/GaBiInSn/nonwoven fabric (LM-P-TENGs) is manufactured. The LM-P-TENGs can be integrated onto fabrics without compromising their breathability, comfortableness, and flexibility. Particularly, LM-P-TENGs efficiently convert the mechanical energy of human limb movements into sustainable electrical energy output. Under the human limb mechanical triggering conditions, LM-P-TENG achieves a champion specific open-circuit voltage up to 900 V, peak short-circuit current density of 43.3 mA/m^2, and high power density of 12.56 W/m^2. This work demonstrates the application potential of room-temperature multiphase soft materials in flexible wearable power sources, while introducing a novel power supply mode for wearable electronics. Additionally, the LM-P-TENGs also present applications in self-powered wearables, medical biosensing systems, human-machine interaction systems, near-eye display systems, etc. for the flexible electronics.

1. Introduction

Liquid metals (LMs) have garnered significant attention in recent years due to their exceptional electrical conductivity [1], remarkable fluidity [2], and low-melting point [3]. These inherent characteristics render them highly promising for a diverse range of applications, including energy harvesting [4,5], soft electronics [6–8], human-machine interfaces [9–11]. The utilization of LMs has particularly advanced the development of flexible [12], stretchable [13], chemically functionalized [14], and printable electronics [15]. While LMs are commonly employed in flexible and stretchable electrodes and portable power supplies, current approaches often require external packaging to prevent leakage and improve circuit reliability. Consequently, existing wearable power supplies based on LMs exhibit limited flexibility and intricate device structures, posing significant challenges for practical applications. To address these limitations,

☆ Prof Zhong Lin Wang, an author on this paper, is the Editor-in-Chief of Nano Energy, but he had no involvement in the peer review process used to assess this work submitted to Nano Energy. This paper was assessed and the corresponding peer review managed by Professor Chenguo Hu, also an Associate Editor in Nano Energy

* Corresponding authors.
E-mail addresses: liangfeiduan1012@163.com (L. Duan), pzhyang@hotmail.com (P. Yang).

https://doi.org/10.1016/j.nanoen.2024.110305
Received 5 August 2024; Received in revised form 8 September 2024; Accepted 25 September 2024
Available online 28 September 2024

researchers have proposed harnessing human movement energy through conversion devices to power wearable electronics [16,17]. In this context, triboelectric nanogenerators (TENGs) have emerged as a competitive solution, offering promising prospects in wearable devices [18,19], self-powered sensing [20–22], and flexible electronics [23–25]. TENGs enable advanced concepts for integrated flexible electronics that prioritize flexibility while ensuring personal safety and environmental sustainability [26,27]. Despite the widespread use of liquid metals in flexible clothing electronics, their flow and ability to permeate open fabric surfaces or unstructured flexible substrates often result in electrical failures during the construction of TENGs or flexible circuits. Recent implementations of biphase liquid metals have allowed for the creation of elastomeric encapsulated circuits and printed electronics with outstanding electrical stability under significant deformations [28,29]. However, achieving desirable performance still necessitates the development of intricate dedicated channels or high-temperature processes. Room-temperature liquid metals (RTLMs), such as GaBiInSn alloys, offer a promising solution to these challenges. These materials exhibit fascinating metallic fluidic properties and multifunctional behaviors, resolving issues faced by conventional technologies and opening new avenues in scientific and engineering research. RTLMs enable rapid and customizable fabrication of wearable electronics and can be directly printed onto flexible substrates, facilitating the formation of conductive layers with excellent stability under deformation.

In this study, we propose an integrated wearable TENG fabricated on a flexible textile substrate by employing room-temperature multiphase GaBiInSn metals for direct printing. We synthesize a multiphase GaBiInSn alloy ($Ga_{33.5}Bi_{16.55}In_{35.9}Sn_{14.0}$) at room temperature, consisting of solid, liquid, and paste phases. This unique composition allows for direct transfer onto the target fabric surface using tape, facilitating the formation of a conductive layer. By depositing a pre-prepared PTFE film layer on the surface of the multiphase GaBiInSn metals/non-woven layer and positioning the top and bottom electrodes, we establish an integrated wearable LM-based TENG (LM-P-TENG). Our device demonstrates remarkable performance, achieving a maximum open-circuit voltage (V_{oc}) of 900 V and a transient power density of 12.56 W/m^2. This work not only advances the field of wearable energy harvesting but also provides potential for diverse applications in human-computer

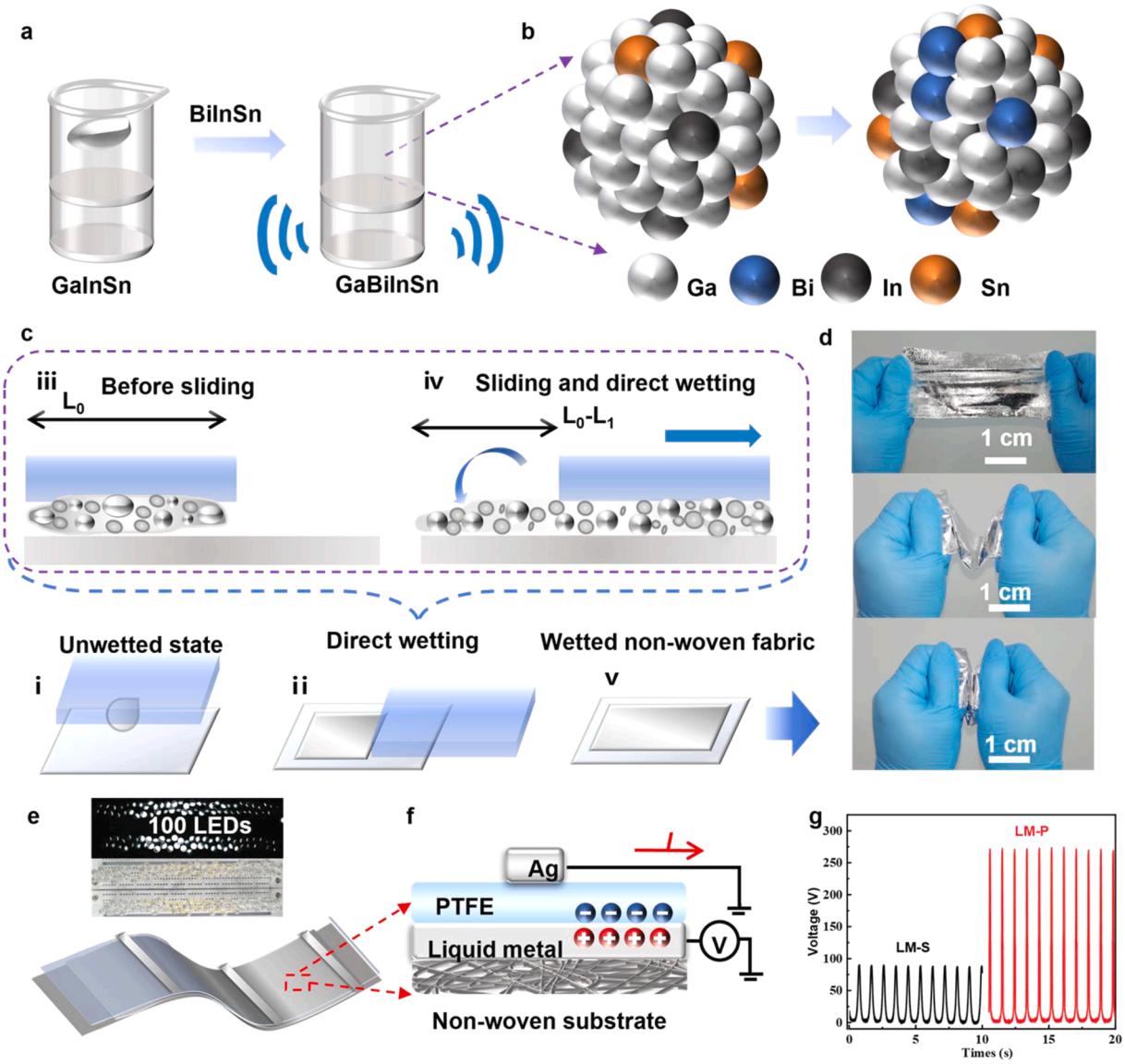

Fig. 1. (a) GaBiInSn manufacturing process. (b) Atomic structures of GaInSn and GaBiInSn. (c) Acrylic-based tape assisted transfer process, and multiphase soft metals/non-woven fabric after printing. (d) Photos of one-sided multiphase soft metals/non-woven fabric under stretching and bending. (e) Structure of an array electrode based TENG. (f) Structural design of LM-P-TENG. (g) V_{oc} of LM-P-TENG.

interfaces, seamlessly integrated wearable electronics, self-triggering sensor devices, and smart homes. By leveraging the unique properties of room-temperature multiphase soft metals, we pave the way for a new generation of high-performance, fabric-based wearable energy harvesting devices.

2. Results and discussion

2.1. Manufacturing LM-P-TENG on flexible fabrics

The high surface energy of LMs often results in their poor wettability on solid substrates, such as non-woven fabric substrates. To overcome this shortcoming posed by the high surface tension of LMs, which hinders their being printed on fabric surfaces, we previously developed room temperature multiphase soft metals to enhance material performance for achieving functional printing and device fabrication of LMs [30]. To prepare the room-temperature multiphase GaBiInSn metals, the $Ga_{67}In_{20.5}Sn_{12.5}$ alloys and $Bi_{33.1}In_{51.3}Sn_{15.6}$ alloys were first mixed with mechanical vibration using a mixer as shown in Fig. 1a. The mechanism diagram in Fig. 1b illustrates a comparison between the atomic structures of the multiphase GaBiInSn metals and the GaInSn alloys, with the liquid metal exhibiting a typical amorphous atomic distribution structure. Meanwhile, the corresponding photo highlights their distinguishing features. It can be observed that drops of $Ga_{67}In_{20.5}Sn_{12.5}$ alloys on non-woven fabric exhibit high reflectance and a uniform metallic appearance, whereas $Ga_{33.5}Bi_{16.55}In_{35.9}Sn_{14.05}$ metals have a rough silver-white appearance (Supplementary Fig. S1). The manufacturing process depicted in Fig. 1c involves the deposition of multiphase soft metal onto the nonwoven fabric via the use of an acrylic-based tape, resulting in the formation of a dense coating. Here, the acrylic-based tape has a typical polymer viscosity, which enables it to adhere to multiphase soft metals. The Supplementary Fig. S2a illustrates the original surface of the acrylic-based tape, as well as the complete coating formed with two types of LMs, as shown in Supplementary Fig. S2b and Supplementary Fig. S2c. Firstly, we use an acrylic tape to easily deposit GaBiInSn coating onto the non-woven fabric through frictional contact. The GaBiInSn metals were immersed in the adhesive surface of the tape, ensuring complete coverage. Subsequently, the surface of the acrylic-based tape, which bears a layer of GaBiInSn metals, is gently attached to the non-woven fabric. To achieve a uniform coating of GaBiInSn metal on the nonwoven surface, we apply certain lateral tension to induce controlled sliding displacement from the acrylic-based tape. As shown in the Fig. 1c(i) to Fig. 1c(iv), the GaBiInSn metal can be smoothly peeled off and simultaneously transferred to the surface of the nonwoven fabric. This phenomenon is attributed to the fluid properties of the multiphase metal, where interfacial sliding friction and capillary action at the solid/liquid/air interface serve as driving forces for the transfer. This lightweight and highly flexible substrate has favorable characteristics, such as being thin enough to fit comfortably on the fingers and allowing for fine bending movements (Supplementary Fig. S3).

Subsequently, a PTFE film with a thickness of 0.03 mm is applied to ensure seamless bonding between GaBiInSn metals and the PTFE film under ambient temperature and pressure conditions. Additionally, a polyimide (PI) tape is utilized to seal the edges in order to prevent electrical leakage. An Ag electrode is attached onto the surface of PTFE. The resulting device structure is depicted in Fig. 1e where both top and bottom electrodes are interconnected forming a loop for the monitoring purposes using a voltmeter. Additionally, the incorporation of parallel Ag electrodes on the surface of PTFE can effectively enhance energy harvesting capabilities and eliminate the need for intricate wire connections to achieve an array output, as depicted in Fig. 1f. The results demonstrate that this LM-P-TENG design effectively generates V_{oc} of 285 V that can simultaneously drive 110 LEDs (Rated power of 0.06 W) (Fig. 1e and Supplementary Video S1). Compared with the conventional approaches, this strategy obviates the need for fabricating fully enclosed or patterned conductive layers and for constructing intricate electrical interconnections.

2.2. Material characteristics

To achieve a uniform coverage of the multiphase GaBiInSn metal on non-woven substrates, it is essential to consider the interfacial interaction and the difference in wettability between the multiphase GaBiInSn metal and non-woven fabric substrates. The eGaInSn exhibits typical liquid properties, whereas the BiInSn alloys remains solid state due to its higher melting point, which indicates that multiphase GaBiInSn metals may possess different characteristics compared with the GaInSn and BiInSn alloys (Fig. 2a). To further explain the mechanism behind this, we tested the interfacial interaction and performance of the multiphase GaBiInSn metal and eGaInSn on non-woven fabrics. The GaInSn alloy droplets exhibit a tendency to roll and rapidly detach from non-woven fabric substrates at an inclination angle of 45° (Fig. 2b(i–ii), Supplementary Fig. S4 and Supplementary Video 2). We further conducted the obliquity experiment and observed that the droplet of the multiphase GaBiInSn metal exhibited strong interfacial adhesion to the non-woven fabric substrate, preventing it from rolling off even at an inclination of 80° (Fig. 2b(iii–iv) and Supplementary Video 3). This approach demonstrates enhanced liquid metal adhesion without the constraints typically associated with physical processing methods, setting it apart from previously reported techniques [31–35]. The improved results can likely be attributed to the unique interfacial interaction between the multiphase GaBiInSn alloy and the non-woven fabric substrate, which significantly contributes to the stability and durability of the printed structures.

Moreover, to investigate the influence of bismuth (Bi) content, GaBiInSn metals were synthesized with varied compositions ranging from $Ga_{67}In_{20.5}Sn_{12.5}$ to $Ga_{16.75}Bi_{24.83}In_{43.6}Sn_{14.82}$, and the morphologies of GaBiInSn metals with different atomic ratios were examined, as shown in Fig. 2. It is evident that the surface of GaInSn is very smooth (Fig. 2c), whereas the GaBiInSn metals (Fig. 2d) displays a relatively rough surface. Moreover, in the GaBiInSn metals, a distinct multiphase structure is formed consisting of solid phase, liquid phase, and paste phase, which are uniformly distributed, as shown in Fig. 2e-g. The amount and size of crystal nucleus increased as the atomic ratio of bismuth increased from 16.55 % to 24.83 %. The Energy Spectrum Scanning (EDS) results show the coexistence of Ga, In, Bi, and Sn elements, demonstrating their good dispersion and uniform distribution.

The crystal particles were interconnected by a liquid-bridge, resulting in the retained liquid/solid mixture characteristic of the multiphase GaBiInSn metal. Furthermore, the effect of the printable characteristic of different multiphase GaBiInSn metals on the non-woven fabric substrate was also investigated, as shown in Supplementary Fig. S5. The surface of the $Ga_{67}In_{20.5}Sn_{12.5}$ alloy exhibits a reflective appearance with significant areas of unprinted perforations, while the surface of the $Ga_{33.5}Bi_{16.55}In_{35.9}Sn_{14.05}$ metal forms a fully coated layer without any voids. Similarly, the Scanning Electron Microscope (SEM) image reveals distinct micron-scale perforations when the $Ga_{67}In_{20.5}Sn_{12.5}$ alloy is printed on a silver fabric substrate (Supplementary Fig. S6), and intermittent blank regions are observed when its being printed on a non-woven fabric substrate (Supplementary Fig. S7). This phenomenon can be attributed to the high surface tension and fluidity of the $Ga_{67}In_{20.5}Sn_{12.5}$ alloy, resulting in inadequate wettability towards non-woven fabrics and leading to discontinuous printing areas.

Meanwhile, the multiphase characteristics of the $Ga_{33.5}Bi_{16.55}In_{35.9}Sn_{14.05}$ metal are still retained on the non-woven substrate, as confirmed by X-ray Crystal Diffraction (XRD) that indicates an amorphous structure for the $Ga_{67}In_{20.5}Sn_{12.5}$ alloy and a multiphase structure for the $Ga_{33.5}Bi_{16.55}In_{35.9}Sn_{14.05}$ metal (Supplementary Fig. 8). The presence of crystal phases can be attributed to embedded BiInSn free metal particles in the $Ga_{67}In_{20.5}Sn_{12.5}$ alloy, while XPS results demonstrate varying degrees of oxidation (Fig. 2h-k).

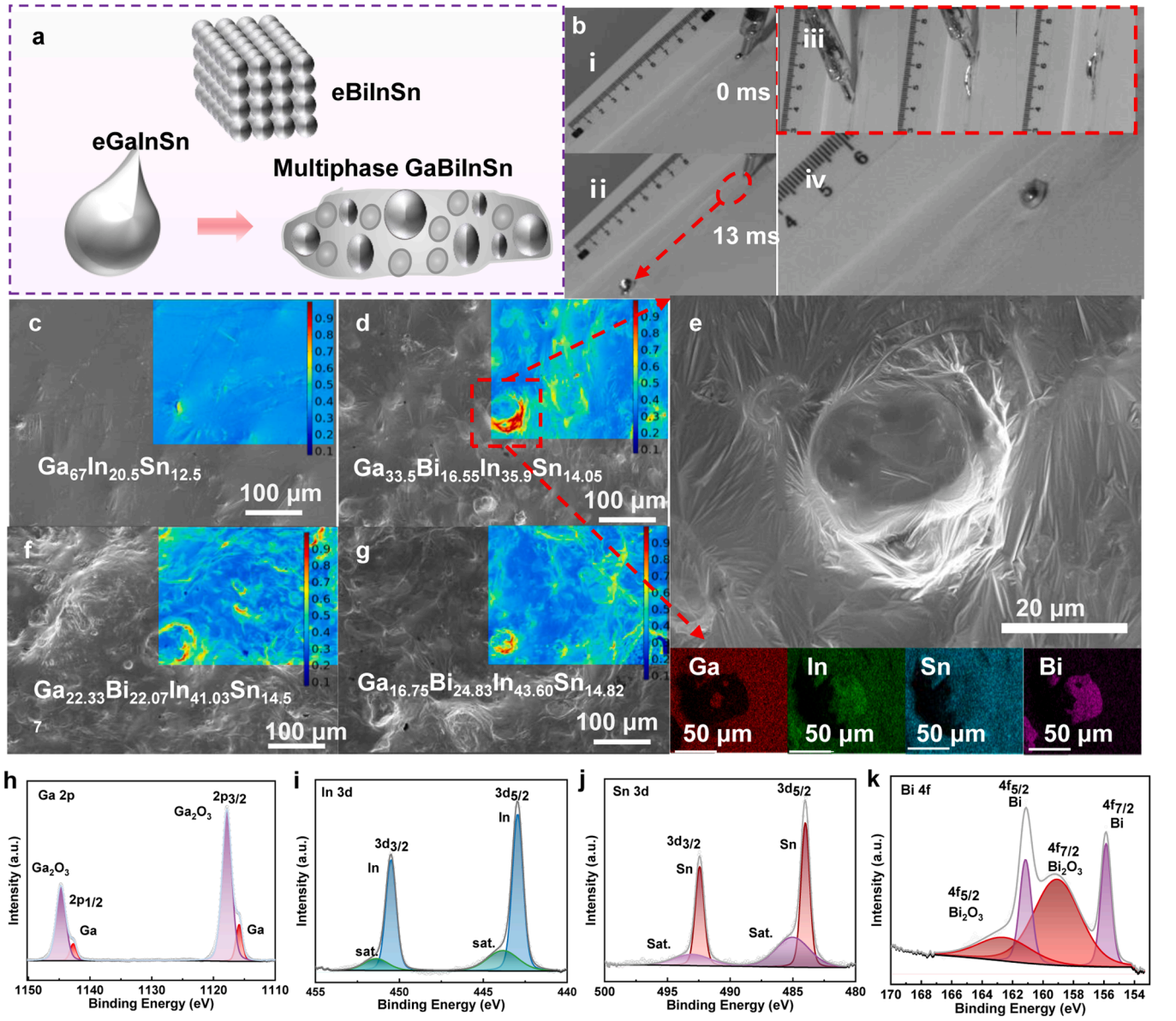

Fig. 2. (a) Schematics of different types of alloys. (b) Dynamic contact angle testing. (c-g) SEM images of multiphase GaBiInSn metals after printing, the insets of (e) show the corresponding EDS mapping of Ga, Bi, In and Sn elements. (h-k) XPS results for multiphase GaBiInSn metals.

The spatial distribution of liquid metal clusters influences the capillary effect at the solid-liquid interface between metal particles, thereby enhancing their wettability on the substrate [36].

2.3. Electrical output of LM-P-TENG

The structure of this LM-P-TENG and its corresponding cross-sectional view are shown in Fig. 3a and Fig. 3b. The LMs and PTFE film resembles the formation of a solid-liquid interface. The capacitance equivalent to the PTFE/LMs interaction is denoted as C_{LM}, where C_1 represents the equivalent capacitance at the solid/PTFE film contact interface and C_2 denotes the flat plate capacitance formed by the top electrode/LMs combination. According to the established equivalent circuit model, a fundamental system loop can be derived (Fig. 3c). However, effectively separating the triboelectric charges from the solid-liquid interface poses a significant challenge due to the EDL (electric double layer) ability to shield interface charges. We proposed the mechanism of the LM-P-TENG, as shown in Fig. 3d. Initially, when there is no contact between the Cu layer and the Ag/PTFE interface, the system is in an electrostatic shielding state. Next, when the Cu conductor comes into contact with the Ag/PTFE interface on the surface of the TENG, a closed loop is formed and the stored charge is released, resulting in electron flow from the Ag to the LMs. Eventually, upon the separation of Cu, a reverse electron flow is induced from LMs to Ag, thereby completing the power generation cycle. The corresponding output performance of TENG through contact/separation is observed, generating a V_{oc} of 280 V, I_{sc} of 10 μA and Q_{sc} of 150 nC (Fig. 3e-g).

As depicted in Fig. 3h, the V_{oc} amplification signal demonstrates that at t_1, which marks the moment of contact initiation, the voltage rapidly increases to its maximum value. Subsequently, as time progresses and t_2 signifies the separation between the copper friction layer and Ag/PTFE interface, the voltage returns to zero. The negative voltage observed after t_2 is attributed to electron reflux and redistribution of electric charge on surface of PTFE, thereby influencing subsequent power generation cycles. The identical peak characteristics of the transient current also serve as evidence for the electron transfer cycle in the mechanism, as depicted in Fig. 3f and Fig. 3i. A detailed analysis of the time scale associated with the amplified current signal across various TENG modes

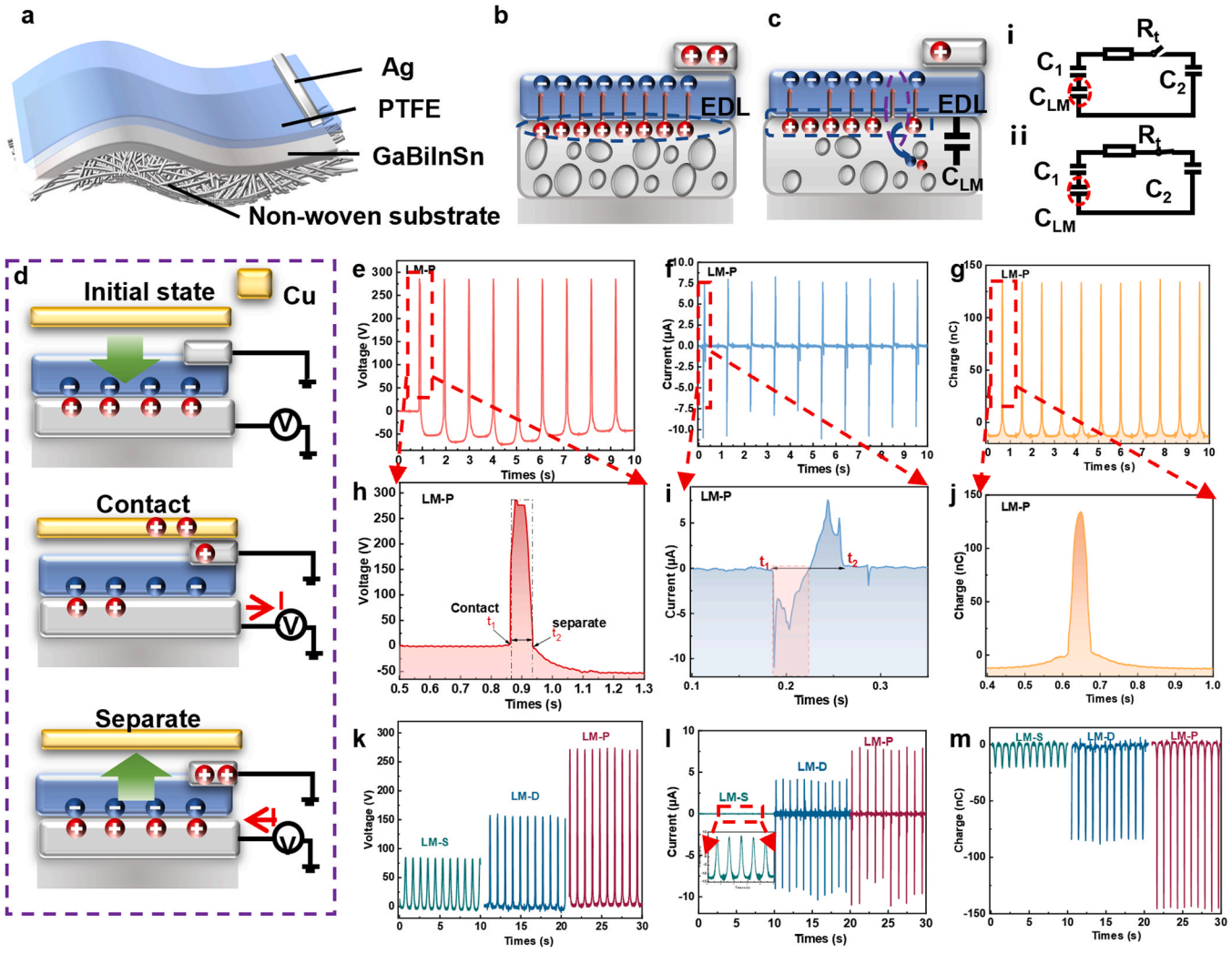

Fig. 3. (a) Device structure diagram of LM-P-TENG. (b-c) Charge storage mechanism and equivalent circuit diagram of electrode in LM-P-TENG. (d) Electron transfer mechanism of TENG. (e-j) V_{oc}, I_{sc}, and Q_{sc} of LM-P-TENG and corresponding single amplified signal. (k-m) The V_{oc}, I_{sc}, Q_{sc} of different TENG modes.

is provided in Supplementary Fig. 9, demonstrating that the LM-P-TENG exhibits a notably shorter time scale (up to 0.038 s) compared to both the LM-S and LM-D modes, thereby underscoring its superior current output performance. The alternating current (AC) signal characteristics are indicated by the negative and positive cycles observed from t_1 to t_2, with a corresponding charge transfer amount of 133.5 nC (Fig. 3g and Fig. 3j). Then, the electrical experiments of single-electrode mode TENG were designed in bending (Supplementary Fig. 10) and stretching modes (Supplementary Fig. S11) for comparison, which exhibit similar longer time scales characterized by slow deformation to produce electrical output changes. These results indicate that LM-P-TENG differs from output modes of LM-S-TENG. To further investigate the impact of this type of TENG on electrical output in different environments, we conducted experiments at room temperature (25 °C) as well as lower temperatures (0 °C). The results indicate that the performance of both $Ga_{67}In_{20.5}Sn_{12.5}$ alloys and $Ga_{33.5}Bi_{16.55}In_{35.9}Sn_{14.05}$ based LM-P-TENG decreases with temperature. However, when comparing $Ga_{67}In_{20.5}Sn_{12.5}$ alloys to $Ga_{33.5}Bi_{16.55}In_{35.9}Sn_{14.05}$ metal-prepared TENG, it is observed that $Ga_{67}In_{20.5}Sn_{12.5}$ alloys exhibits superior V_{oc}, I_{sc}, and Q_{sc} characteristics due to its enhanced charge-capture capability and interfacial stability resulting from its multiphase structure (Supplementary Fig. 12).

In order to comprehend the energy harvesting characteristics of the liquid metal flexible TENG, we devised single-electrode mode TENG (LM-S-TENG) and double-electrode mode TENG (LM-D-TENG), as depicted in Supplementary Fig. 13 The performance of LM-S-TENG, LM-D-TENG and LM-P-TENG was compared, as presented in Fig. 3k-m. Among the three types of TENG, the LM-P-TENG device achieved the highest values for V_{oc} of 285 V, I_{sc} of 10 μA, and Q_{sc} of 150 nC, indicating significantly enhanced output performance. The waveform of this electrical signal is pulsed, indicating that the transfer of electrons is associated with periodic motion during contact separation [37,38] The generation processes of LM-S-TENG and LM-D-TENG differ from that of LM-P-TENG in that the maximum induced charge occurs at the moment of contact/separation between the friction layers, where the changing electric field propels electron motion, thus making current amplitude dependent on contact/separation speed.

To further investigate the effects of the contact area on the LM-P-TENG performance, we systematically varied the contact area of the Cu layer to be 7.5 cm^2, 3.25 cm^2, and 1.63 cm^2, respectively. We ensured that the Cu layer always contacted with the central region of the Ag electrode on the surface of PTFE. As depicted in the Fig. 4a-c, the reduction of the area from 7.5 cm^2 to 1.63 cm^2 leads to a decrease in the C_1 and subsequent decline in the output of LM-P-TENG, displaying V_{oc}, I_{sc} and Q_{sc} from 270 V, 8 μA, and 170 nC to 125 V, 7 μA, and 70 nC, respectively.

We also investigated the impact of the quantity of surface electrodes on the output performance of LM-P-TENG. The increase in the number of

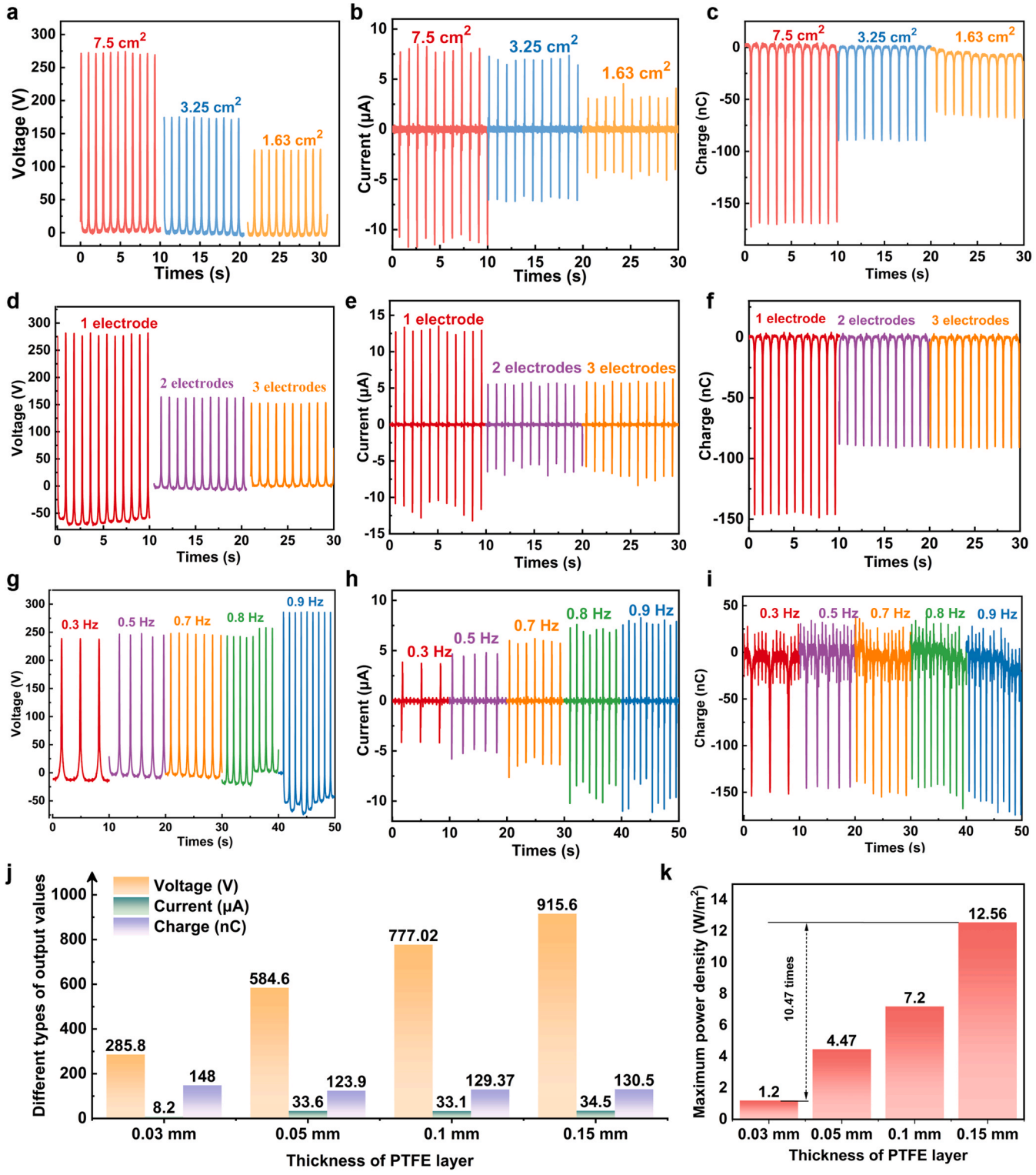

Fig. 4. Effects of contact area between Cu friction layer and TENG on output performance: (a) V_{oc}, (b) I_{sc}, and (c) Q_{sc}. The effects of the number of electrodes in LM-P-TENG in fixed electrode mode on (d) V_{oc}, (e) I_{sc} and (f) Q_{sc}; The output of (g) V_{oc}, (h) I_{sc}, and (i) Q_{sc} of LM-P-TENG at various frequencies. (j) The voltage output by different types of TENG along with the number of cycles. (j) The output values of V-I-Q and (k) the maximum power density of LM-P-TENG with PTFE of thickness ranging from 0.03 mm to 0.15 mm.

top electrodes from 1 to 3 for LM-P-TENG led to a reduction in V_{oc} amplitude from 300 V to 150 V, as depicted in Fig. 4d-f. Furthermore, there was a decrease in current from 12.5 μA to 5 μA and a decline in transferred charge from 145 nC to 90 nC. Similar outputs were observed for LM-P-TENG with both 2 and 3 of top electrodes. We attribute this phenomenon to the presence of a parasitic capacitance at the interface between the top electrode and the PTFE layer. The addition of parallel top electrodes of equal size can cause a capacitance bridging effect, following the formula $C = C_1 + C_2 + \ldots + C_n$. This increase in coupled capacitance results in a reduction in transferred charge quantity,

consequently diminishing the output power of LM-P-TENG.

Furthermore, the output performance of LM-P-TENG is affected by the external excitation frequency. We conducted tests on the output performance of LM-P-TENG within a range of 0.3 Hz to 0.9 Hz for V_{oc} (Fig. 4g), I_{sc} (Fig. 4h) and Q_{sc} (Fig. 4i). Notably, both V_{oc} and Q_{sc} exhibited steady but gradual increases in amplitude with increasing frequency, reaching maximum outputs ranging from 240 V (at 0.3 Hz) to 275 V (at 0.9 Hz). The I_{sc} also increased with frequency, ranging from 0.3 Hz to 0.9 Hz, which may be due to an accumulation of bound charges at higher frequencies resulting in increased transferred charge.

We also compared the output performance of the TENG at frequencies of 1–5 Hz, and found that as the frequency increased, the open-circuit voltage showed an upward trend, ranging from 285 V to nearly 312 V (Supplementary Fig. S14a-c). The current exhibited a quasi-DC characteristic (with a downward trend in the positive half-axis peak value and an increasing trend in the amplitude of the negative half-axis current). By further comparing the charge transfer rates at 1 Hz and 5 Hz frequencies, we can see that the average charge transfer rate per second decreased from 228 nC/s at 1 Hz to 61 nC/s at 5 Hz, indicating an increasing trend in the total charge transfer but a decreasing trend in the average charge transfer rate (Supplementary Fig. S14d-f). The long-term stability of the TENG was tested for 6 months, as illustrated in the Supplementary Fig. S15, where a stable output of V_{oc} is evident, thereby demonstrating its exceptional robustness.

In contrast to the high fluidity of eGaInSn, the coating of multiphase GaBiInSn metals on non-woven fabrics exhibits improved peel resistance

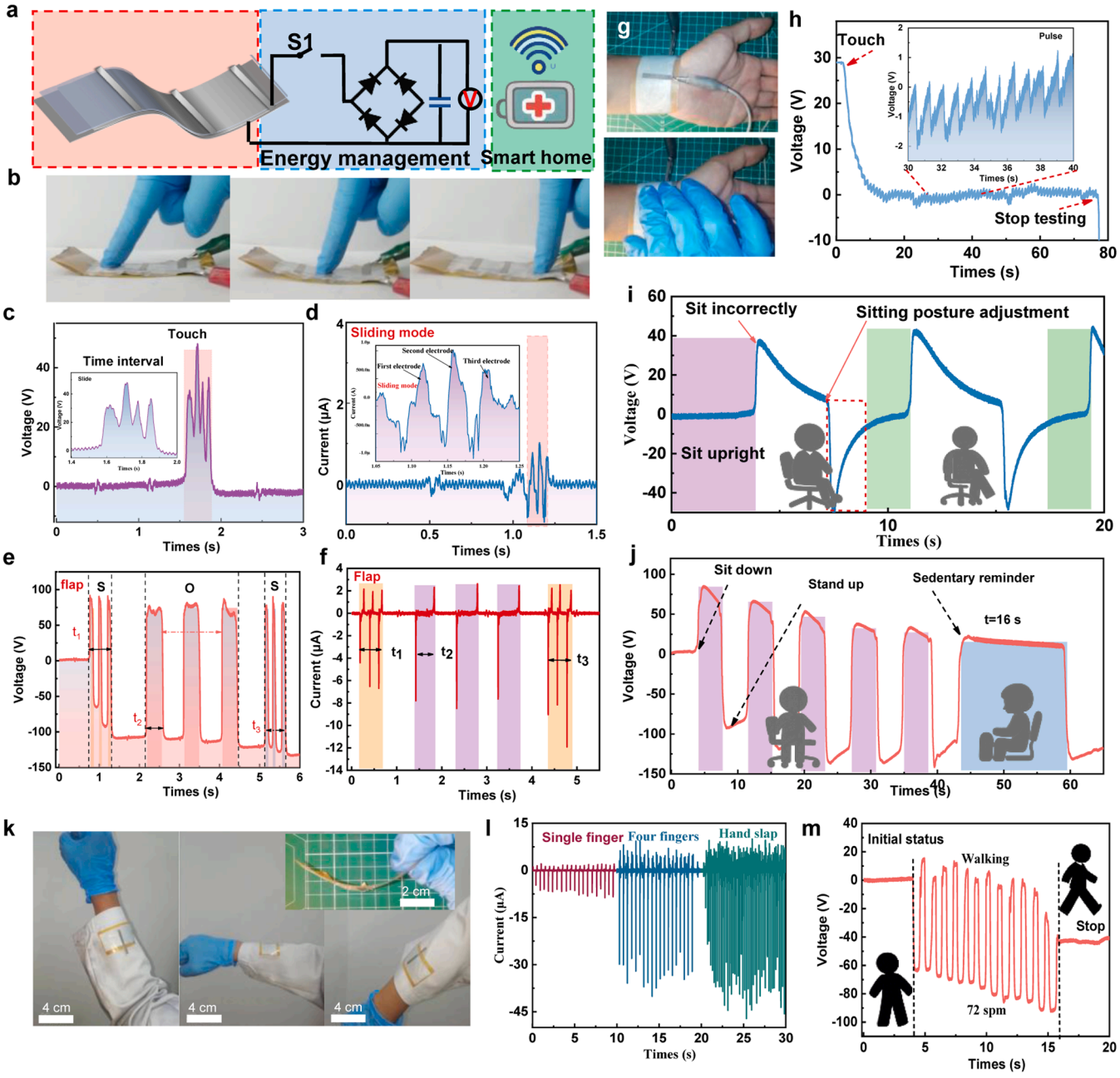

Fig. 5. (a) The power management circuit of LM-P-TENG, (b) An image of the finger sliding over the three top electrodes, (c)The voltage signal and (d) current amplified signal when finger moves across the three top electrodes, (e) The voltage signal of the "SOS" code and (f) the current signal, (g) TENG is used for measuring pulse scenarios and (h) the corresponding voltage signals, (i) the voltage signal of the TENG monitoring the sitting position of user and (j) the output voltage signal of the sedentary reminder function, (k) Photos of flexible TENG integrated with clothing, (l) Output current driven by hand tapping TENG, (m) Voltage signal for walking monitoring.

and leak resistance. This enhances the charge transfer ability at the interface between PTFE and GaBiInSn layers (Supplementary Fig. S16), ultimately resulting in superior output performance for LM-P-TENG. The load characteristics of the LM-P-TENG were then investigated (When the thickness of the PTFE film is 0.03 mm). As shown in Supplementary Fig. S17a, a maximum V_{oc} of 285 V was achieved at a load resistance of 1 GΩ through applying the maximum power transfer theorem $P=I^2R/S$ (Where R represents resistance and S represents effective area), and the corresponding peak power was determined to be 900 μW (Supplementary Fig. S17b).

In the structure of LM-P-TENG in this work, the electrical performance of the generator is adjustable and optimized, for this, we supplemented experimental verification, as shown in Fig. 4j and Supplementary Fig. S18a-c, we discussed the influence of PTFE dielectric layer thickness on the output performance of TENG, and found that as the thickness of the PTFE dielectric layer increased from 0.05 mm to 0.15 mm, the effective V-Q-I were improved, this may be attributed to the electret properties of PTFE, resulting in an increase in thickness resulting in an increase in electrical output. Similarly, as shown in Fig. 4k, the power density of the LM-P-TENG made of PTFE with a thickness of 0.03 mm is also increased compared to the one made of PTFE with a thickness of 0.5 mm to 0.15 mm, respectively, were 4.47 W/m^2, 7.2 W/m^2, and 12.56 W/m^2 (Supplementary Fig. S18d-f), Compared to the recently reported TENG, it exhibits impressive performance (Supplementary Table S1).

To demonstrate the potential of this TENG for wearable power supply, we have developed a TENG with three top electrodes arranged in a parallel array structure, as illustrated in Fig. 5a. This device operates by utilizing the electrical signal generated when the finger or palm comes into contact with the electrode on the LM-P-TENG surface as a pulse signal for gesture recognition, thereby enabling the creation of a self-powered human-computer interaction interface. Furthermore, to manage the energy output of the LM-P-TENG, we employed a rectifier bridge circuit and controlled charging of the capacitor connected to its output end by a switch1 (S1). meanwhile, its charging voltage could be monitored using a voltmeter. However, due to capacitive coupling effect among them, there is no need for overall interconnection between these three top electrodes; only one electrode needs to be connected to complete the loop. The rectified voltage signals are depicted in Supplementary Fig. S19a, with the peak voltage reaching values of 280 V. And, the charging capability of the TENG is assessed through the energy management circuit. As depicted in Supplementary Fig. S19b, different capacitors result in varying charging voltages by the TENG device, and all voltage curves exhibit a step-like increase within 30 s, indicating an accelerated charging capability.

Moreover, to explore applications involving gesture-based human-computer interaction (Fig. 5b), we placed three parallel Ag electrodes on PTFE surface with a spacing of 3 cm. To simulate finger sliding triggering of TENG, we sequentially tested finger sliding across these three electrodes which generated dense spiking voltage and current signals, as illustrated in Fig. 5c and Fig. 5d, respectively, accurately reflecting temporal states. The magnified signal set reveals that each spike corresponds to finger contact/departure time from its respective electrode. The TENG device was subsequently showcased as a viable emergency power source. As depicted in Fig. 5e and Fig. 5f, users can effortlessly generate voltage signals with a relative amplitude of 150 V and current signals with a relative amplitude of 10 μA by simply making a contact with the top electrode using their finger. This value is higher than those reported for TENG devices with similar functions [39,40]. The serial pulses, characterized by “long time” or “short time” contact/separation interactions within a specific time interval, can effectively represent “SOS” messages in Morse code. Then we also implemented a scenario that mimics the measurement of pulse signals by traditional Chinese medicine palpation, as shown in Fig. 5g and h. We covered the bottom of the TENG with the hand area and placed the top electrode region in contact with the external finger. By maintaining close contact, we could collect pulse signals (Fig. 5h). When the voltage signal stabilized, a spike-shaped output signal was generated (approximately 1.6 V).

Additionally, it can also be applied in the scenario of working from home, such as posture monitoring, because the flexible TENG can be integrated into clothing worn all over the body, as shown in Fig. 5i. When the human posture is correct, no signal is generated at this time. However, when the back presents a “hunchback” state, the TENG on the back will immediately trigger a 40 V voltage signal. When the posture is restored to the sitting position, the TENG generates the next signal cycle; at the same time, it also has the function of reminding long sitting, as shown in Fig. 5j. When the person sits down, the TENG immediately generates a voltage signal exceeding 50 V, and as the number of cycles increases, the voltage amplitude exceeds 150 V in response, thus clearly distinguishing the sitting and standing states. When the TENG detects that the sitting time exceeds the threshold value, for example (t=16 s), it begins to alarm, thus achieving the effect of reminding long sitting.

Finally, the wearable flexibility of the LM-P-TENG was demonstrated in Fig. 5k, showing that it can be well integrated with clothing. Then, we found that TENG exhibits a coupling effect when triggered by the human body, as shown in Fig. 5i. When the output current amplitude increased as the single finger, four fingers, and palm of the hand were in contact with the TENG surface (Supplementary Video S4). Interestingly, the device can also be used to monitor the initial, walking, and stopping states of the human body, so the walking frequency can be counted and analyzed by the voltage signal (Fig. 5m), and the single output voltage amplitude exceeds 60 V. This result indicates that the larger contact area enhances charge transfer due to the increased capacitive coupling between the effective charging area of the human body and the TENG, resulting in higher voltage and current responses. The above results demonstrate the potential for the TENG prepared in this work to have flexible, flexible, and wearable seamless integration for self-powered scenarios.

3. Conclusion

In this study, we have successfully developed an innovative in-situ method for constructing friction-based nanogenerators on textile substrates using liquid metals (LMs). This approach leverages the unique mixed-phase properties of multiphase liquid metals to create a conductive layer on non-woven fabric substrates, a feat previously challenging to achieve. Our liquid metal-based PTFE triboelectric nanogenerator (LM-P-TENG) demonstrates impressive electrical performance, achieving an V_{oc} of 900 V, a I_{sc} of 32.5 μA, and a transfer charge of 145 nC. This novel technique offers exceptional flexibility and ease of manufacturing, overcoming limitations present in similar devices. We have showcased its practical applications, including device arraying, energy management and storage, simple gesture touch and slide recognition, and its potential as a self-powered emergency power source. The significance of this work extends beyond its immediate applications. By integrating advanced fabrication processes with flexible printing materials, future iterations of these TENG devices could see further enhancements in both sensing capabilities and energy conversion and storage performance. This opens up extensive prospects for applications in flexible human-computer interaction, wearable electronic devices, and self-powered sensing systems. The method used in this work is compatible with commercial flexible printing technology, has a wide compatibility with substrates and manufacturing processes, is not limited by the size and shape of the substrate, and therefore has wide applicability and lower cost, which is helpful for mass production in the future.

4. Methods

4.1. The preparation of room-temperature multiphase GaBiInSn metals

The Ga, In, Sn were purchased from Shanghai Aladdin Company,

while the $Bi_{33.1}In_{51.3}Sn_{15.6}$ alloys (with a melting point of 60 ℃) was obtained from Yunnan Zhongxuan Liquid Metal Technology Co., LTD. Firstly, Ga, In and Sn metal particles were mixed in a mass ratio of 67:20.5:12.5 to obtain the $Ga_{67}In_{20.5}Sn_{12.5}$ alloys (with a melting point of 10 ℃). The alloys was then weighed according to the mass ratio and mixed with $Bi_{33.1}In_{51.3}Sn_{15.6}$ alloys using a mechanical vibration mixer for 10 min to prepare the $Ga_{67}In_{20.5}Sn_{12.5}$ metals. The mixture was then heated to 70 ℃ for 24 h under argon protection. Subsequently, the resulting GaBiInSn were sealed in sample bottles and stored for future use. Non-woven fabric was purchased from Beijing Labgic Technology Co, LTD, while PTFE film, acrylic-based tape, copper tape and silver cloth tape were acquired from Alibaba Group. The TENG electrodes are interconnected through a conductive silver cloth, forming a closed loop. The TENG was driven by a linear motor with operating frequency of 0.9 Hz, and the output voltage, current and charge were measured.

4.2. Preparation of TENG

The preparation of PTFE film: A piece of PTFE film cut into 3 cm×2.5 cm, was utilized as the moving friction layer and subjected to ultrasonic cleaning with deionized water for 10 min, followed by drying with nitrogen gas.

Preparation of LM-S-TENG: The prepared PTFE film was used as the moving friction layer, and a printed liquid metal layer/non-woven material was employed as the friction interface. The output end of the single electrode mode was connected to a conductive silver cloth for charge collection.

Preparation of LM-D-TENG: the prepared PTFE film served as the moving friction layer which has a polytetrafluoroethylene film on its backside embedded with copper electrodes. The relative friction layer consisted of a liquid metal layer/non-woven material, where both copper electrodes and liquid metal layers were separately connected to form a contact separation mode TENG.

Preparation of LM-P-TENG preparation: Cu film was used as the moving friction layer, while the top surface of liquid metal layer/non-woven material was covered with a packaged PTFE film, And use PTFE film with thicknesses of 0.03, 0.05, 0.1, and 0.15 mm as the friction layer. Additionally, linear silver electrodes (5 cm ×0.2 cm) were arranged on top of PTFE so that Ag electrode and liquid metal layers were individually connected to form an LM-P-TENG. The copper conductor acts as the moving friction layer and is driven by a linear motor for reciprocating movement. The Ag electrode on the surface of the TENG acts as the top electrode, the liquid metal printed layer/non-woven fabric acts as the bottom electrode, and the Ag electrode and liquid metal act as the working electrode. When the copper conductor contacts Ag/PTFE, the copper /Ag and liquid metal layer form an equivalent closed loop to produce output.

4.3. Measurements and characterizations

The Scanning Electron Microscopy (SEM) tests were conducted using a Zeiss Sigma300 instrument. Energy Spectrum Scanning (EDS) tests were performed with an Oxford Xplore30 system. X-ray Photoelectron Spectroscopy (XPS) tests were carried out using a Thermo Fisher Scientific K-Alpha+ instrument. X-ray Crystal Diffraction (XRD) analysis was performed on a SmartLabSE device equipped with Cu Ka1 radiation at 40 kV and 50 mA, covering a scan range from 5° to 90°. The V_{oc}, I_{sc} and Q_{sc} of TENG were characterized using an electrometer (Keithley 6514).

CRediT authorship contribution statement

Yong Zhang: Writing – review & editing, Supervision. **Yunbo Zhang:** Resources, Methodology, Conceptualization. **Qin Wang:** Supervision, Resources, Methodology, Conceptualization. **Wen Yang:** Resources, Methodology. **Peizhi Yang:** Writing – review & editing, Supervision, Conceptualization. **Zhong Lin Wang:** Writing – review & editing, Supervision. **Liangfei Duan:** Writing – review & editing, Conceptualization. **Jiangtao Guo:** Writing – original draft, Investigation, Formal analysis, Data curation.

Declaration of Competing Interest

The authors declare that they have no known competing financial interests or personal relationships that could have appeared to influence the work reported in this paper.

Data Availability

Data will be made available on request.

Acknowledgements

This work was funded by the National Natural Science Foundation of China Projects (62465019), Yunnan Province University Service Key Industry Science and Technology Special Projects, Yunnan Yunling Scholars Project, Yunnan Revitalization Talent Support Program; Spring City Plan: the High-level Talent Promotion and Training Project of Kunming (2022SCP005). Yunnan Industrial Technology Innovation Reserve Talent Project (202105AD160056). Yunnan Fundamental Research Projects (202301AU070142, 202401AT070306), the Key Applied Basic Research Program of Yunnan Province (202201AS070023), Yunnan Local University Joint special funds for basic research (202101BA070001–161), the PhD Starting Fund program of Yunnan Normal University (2021ZB005, 01100205020503225). Authors thank the Electron Microscopy Center, the Advanced Analysis and Measurement Center of Yunnan University for the sample testing service.

Appendix A. Supporting information

Supplementary data associated with this article can be found in the online version at doi:10.1016/j.nanoen.2024.110305.

References

[1] D. Wang, J. Ye, Y. Bai, F. Yang, J. Zhang, W. Rao, J. Liu, Liquid metal combinatorics toward materials discovery, Adv. Mater. 35 (2023) 2303533.
[2] J. Gao, J. Ye, S. Chen, J. Gong, Q. Wang, J. Liu, Liquid metal foaming via decomposition agents, ACS Appl. Mater. Inter. 13 (2021) 17093–17103.
[3] N.D. Orf, I.D. Baikie, O. Shapira, Y. Fink, Work function engineering in low-temperature metals, Appl. Phys. Lett. 94 (2009) 113504.
[4] Z. Li, B. Xu, J. Han, D. Tan, J. Huang, Y. Gao, H. Fu, Surface-modified liquid metal nanocapsules derived multiple triboelectric composites for efficient energy harvesting and wearable self-powered sensing, Chem. Eng. J. 460 (2023), 141737-141737.
[5] W. Tang, T. Jiang, F.R. Fan, A.F. Yu, C. Zhang, X. Cao, Z.L. Wang, Liquid-metal electrode for high-performance triboelectric nanogenerator at an instantaneous energy conversion efficiency of 70.6, Adv. Funct. Mater. 25 (2015) 3718–3725.
[6] Do. Hoon Lee, T. Lim, Jeongsu Pyeon, H. Park, S. Lee, S. Lee, W. Kim, M. Kim, J. Lee, D. Kim, S. Han, H. Kim, S. Park, Y. Choi, Self-mixed biphasic liquid metal composite with ultra-high stretchability and strain-insensitivity for neuromorphic circuits, Adv. Mater. 36 (2024) 2310956.
[7] Y.-G. Park, Y.W. Kwon, C.S. Koh, E. Kim, D.H. Lee, S. Kim, J. Mun, Y.-M. Hong, S. Lee, J.-Y. Kim, J.-H. Lee, H.H. Jung, J. Cheon, J.W. Chang, J.-U. Park, In-vivo integration of soft neural probes through high-resolution printing of liquid electronics on the cranium, Nat. Commun. 15 (2024) 1772.
[8] M. Jiang, S. Chen, P. Zhang, Y. Sun, J. Ye, Y. Deng, L. Li, J. Liu, Liquid metal enabled plant injectable electronics, Mater. Today 66 (2023) 50–61.
[9] L. Duan, Y. Zhang, J. Zhao, J. Zhang, Q. Li, Q. Lu, L. Fu, J. Liu, Q. Liu, New strategy and excellent fluorescence property of unique core–shell structure based on liquid metals/metal halides, Small 18 (2022) 2204056.
[10] S. He, J. Dai, D. Wan, S. Sun, X. Yang, X. Xia, Y. Zi, Biomimetic bimodal haptic perception using triboelectric effect, Sci. Adv. 10 (2024) eado6793.
[11] X. Li, M. Jiang, Y. Du, X. Ding, C. Xiao, Y. Wang, Y. Yang, Y. Zhuo, K. Zheng, X. Liu, L. Chen, Y. Gong, X. Tian, X. Zhang, Self-healing liquid metal hydrogel for human–computer interaction and infrared camouflage, Mater. Horiz. 10 (2023) 2945–2957.

[12] S. Li, H. Zhao, H. Xu, H. Lu, P. Luo, T. Zhou, Ultra-flexible stretchable liquid metal circuits with antimicrobial properties through selective laser activation for health monitoring, Chem. Eng. J. 482 (2024) 149173.
[13] S. Chen, S. Fan, J. Qi, Z. Xiong, Z. Qiao, Z. Wu, Joo Chuan Yeo, Chwee Teck Lim, Ultrahigh strain-insensitive integrated hybrid electronics using highly stretchable bilayer liquid metal based conductor, Adv. Mater. 35 (2022) 2208569.
[14] Z. Huang, M. Guan, Z. Bao, F. Dong, X. Cui, G. Liu, Ligand mediation for tunable and oxide suppressed surface gold-decorated liquid metal nanoparticles, Small 20 (2024) 2306652.
[15] L. Duan, Y. Zhang, J. Zhao, J. Zhang, Q. Li, Y. Chen, J. Liu, Q. Liu, Unique and excellent paintable liquid metal for fluorescent displays, ACS Appl. Mater. Inter. 14 (2022) 23951–23963.
[16] G. Liu, J.Y. Kim, M. Wang, J.-Y. Woo, L. Wang, D. Zou, J.K. Lee, Soft, highly elastic, and discharge-current-controllable eutectic Gallium-indium liquid metal-air battery operated at room temperature, Adv. Energy Mater. 8 (2018) 1703652.
[17] W. Zang, Y. Wang, W. Wu, J. Yao, X. Hao, B. Yu, D. Wu, P.-F. Cao, Y. Jiang, N. Ning, M. Tian, L. Zhang, Superstretchable liquid-metal electrodes for dielectric elastomer transducers and flexible circuits, ACS Nano 18 (2023) 1226–1236.
[18] W. Yuan, C. Zhang, B. Zhang, X. Wei, O. Yang, Y. Liu, L. He, S. Cui, J. Wang, Z. L. Wang, Wearable, breathable and waterproof triboelectric nanogenerators for harvesting human motion and raindrop energy, Adv. Mater. Technol. 7 (2021) 2101139.
[19] Z. Sun, Y. Hu, W. Wei, Y. Li, Q. Zhang, K. Li, H. Wang, C. Hou, Hyperstable eutectic core-spun fiber enabled wearable energy harvesting and personal thermal management fabric, Adv. Mater. 36 (2023) 2310102.
[20] Y. Wang, C. Zhao, L. Chen, Q. Wu, Z. Zhao, Jing-Jing Lv, S. Wang, S. Pan, M. Xu, Y. Chen, H. Jin, Flexible, multifunctional, ultra-light and high-efficiency liquid metal/polydimethylsiloxane sponge-based triboelectric nanogenerator for wearable power source and self-powered sensor, Nano Energy 127 (2024) 109808.
[21] X. Qu, Z. Liu, P. Tan, C. Wang, Y. Liu, H. Feng, D. Luo, Z. Li, Z.L. Wang, Artificial tactile perception smart finger for material identification based on triboelectric sensing, Sci. Adv. 8 (2022) eabq2521.
[22] K. Zheng, F. Gu, H. Wei, L. Zhang, X. Chen, H. Jin, S. Pan, Y. Chen, S. Wang, Flexible, permeable, and recyclable liquid-metal-based transient circuit enables contact/noncontact sensing for wearable human-machine interaction, Small Methods 7 (2023) 2201534.
[23] W. Tang, T. Jiang, F.R. Fan, A.F. Yu, C. Zhang, X. Cao, Z.L. Wang, Liquid-metal electrode for high-performance triboelectric nanogenerator at an instantaneous energy conversion efficiency of 70.6, Adv. Funct. Mater. 25 (2015) 3718–3725.
[24] S. Chou, Y. Chen, Z. Yan, T. Lu, T. Wu, M. Lu, T. Ko, W. Peng, J. Chen, F. Hsu, S. Chen, C. Chen, Y. Lai, Topological-insulator nanocomposite and graphite-like tribo-charge-accumulating fabric enabling high-performance non-contact stretchable and textile-based triboelectric nanogenerators with robust charge retention, Adv. Energy Mater. (2024) 2402169.
[25] P. Won, C.S. Valentine, M. Zadan, C. Pan, M. Vinciguerra, D.K. Patel, Seung Hwan Ko, L.M. Walker, C. Majidi, 3D printing of liquid metal embedded elastomers for soft thermal and electrical materials, ACS Appl. Mater. Inter. 14 (2022) 55028–55038.
[26] X. Xue, D. Zhang, Y. Wu, R. Xing, H. Li, T. Yu, B. Bai, Y. Tao, M.D. Dickey, J. Yang, Segregated and non-settling liquid metal elastomer via jamming of elastomeric particles, Adv. Funct. Mater. 33 (2022) 2210553.
[27] X. Liu, Q. Wang, S. Zhou, S. Feng, Y. Wei, F. Bu, K. Wang, J. Wang, B. Zhang, C. Guan, Stiffness and interface engineered soft electronics with large-scale robust deformability, Adv. Mater. (2024) 2407886.
[28] G. Li, M. Zhang, S. Liu, M. Yuan, J. Wu, M. Yu, L. Teng, Z. Xu, J. Guo, G. Li, Z. Liu, X. Ma, Three-dimensional flexible electronics using solidified liquid metal with regulated plasticity, Nat. Electron. 6 (2023) 154–163.
[29] Q. Shen, M. Jiang, R. Wang, K. Song, M.H. Vong, W. Jung, F. Krisnadi, R. Kan, F. Zheng, B. Fu, P. Tao, C. Song, G. Weng, B. Peng, J. Wang, W. Shang, M. D. Dickey, T. Deng, Liquid metal-based soft, hermetic, and wireless-communicable seals for stretchable systems, Science 379 (2023) 488–493.
[30] L. Duan, Y. Zhang, J. Zhao, Q. Li, J. Zhang, J. He, J. Liu, Q. Liu, Formation of multiphase soft metal from compositing GaInSn and BiInSn alloy systems, ACS Appl. Electron. Mater. 4 (2022) 112–123.
[31] S. Liu, D.S. Shah, R. Kramer-Bottiglio, Highly stretchable multilayer electronic circuits using biphasic gallium-indium, Nat. Mater. 20 (2021) 851–858.
[32] Y. He, J. You, M.D. Dickey, X. Wang, Liquid-metal transfer from an anode to a cathode without short circuiting, Nat. Chem. Eng. 1 (2024) 293–300.
[33] Y. Wang, L. Chu, S. Meng, M. Yang, Y. Yu, X. Deng, C. Qi, T. Kong, Z. Liu, Scalable and ultra-sensitive nanofibers coaxial yarn-woven triboelectric nanogenerator textile sensors for real-time Gait analysis, Adv. Sci. 11 (2024) 2401436.
[34] B. Yuan, X. Sun, Q. Wang, H. Wang, Direct fabrication of liquid-metal multifunctional paper based on force-responsive adhesion, Cell Rep. Phys. Sci. 4 (2023) 101419.
[35] H. Chang, P. Zhang, R. Guo, Y. Cui, Y. Hou, Z. Sun, W. Rao, Recoverable liquid metal paste with reversible rheological characteristic for electronics printing, ACS Appl. Mater. Inter. 12 (2020) 14125–14135.
[36] M. Zhang, J. Gong, H. Chang, X. Sun, P. Zhang, J. Fu, L. Liu, X. Li, Y. Wang, W. Rao, Bio-inspired differential capillary migration of aqueous liquid metal ink for rapid fabrication of high-precision monolayer and multilayer circuits, Adv. Funct. Mater. 33 (2023) 2215050.
[37] X. Qu, S. Cheng, Y. Liu, Y. Hu, Y. Shan, R. Luo, S. Weng, H. Li, H. Niu, M. Gu, Y. Fan, B. Shi, Z. Liu, W. Hua, Z. Li, Zhong Lin Wang, Bias-free cardiac monitoring capsule, Adv. Mater. (33) (2024) 2402457.
[38] H. Wang, Y. Kurokawa, J. Wang, W. Cai, J. Zhang, S. Kato, Noritaka Usami, Free-standing electrode and fixed surface tiny electrode implemented triboelectric nanogenerator with high instantaneous current, Small 20 (2023) 2308531.
[39] H.-W. Zhou, C. Zhao, Z.-Y. Zhao, J.-C. Jiang, H.-L. Jin, S. Wang, S. Pan, M.-Y. Xu, Y.-H. Chen, H.-M. Jin, Flexible and multifunctional triboelectric nanogenerator based on liquid metal/polyvinyl alcohol hydrogel for energy harvesting and self-powered wearable human–machine interaction, Rare Met. 43 (2023) 1186–1196.
[40] King Yan Chung, B. Xu, D. Tan, Q. Yang, Z. Li, H. Fu, Naturally crosslinked biocompatible carbonaceous liquid metal aqueous ink printing wearable electronics for multi-sensing and energy harvesting, Nano-micro Lett. 16 (2024) 149.

Jiangtao Guo received his B.S. degree in Applied Physics from Shandong University of Science and Technology (Qingdao, China) in 2018. In 2022 he received his M.S. degree in condensed matter Physics from Yunnan Normal University (Kunming, China). He is currently pursuing his Ph.D. at Yunnan Normal University, and his research interests are mainly in the field of hybrid energy harvesting using friction nanogenerators and wearable systems.

Liangfei Duan received his B.S. and M.S. degrees from School Energy and Environment Science (Solar Energy Research Institute) of Yunnan Normal University, Kunming, China, in 2012 and 2015, respectively. He received his Ph.D. degree from Yunnan University, Kunming, China in 2023. After that he joined Yunnan Normal University as a teacher and researcher. His current research interests include developing liquid metals, flexible electronics, renewable energy, and interface chemical engineering.

Wen Yang, associate professor, is currently mainly engaged in research on low-dimensional materials, thin film solar cells, and their multi-energy integration performance.

Wang Qin received her PhD from Yunnan Normal University and is now a senior experimentalist, master's supervisor, focusing on research and applications of nanomaterials and optoelectronic materials.

Dr. Yunbo Zhang obtained his Ph.D. in Tsinghua University, China (2021). Currently, he is a lecture in Yunnan Normal University, China. His work research interests mainly focus on the development of new energy materials and its relationship to the energy storage devices like lithium ion batteries and zinc ion batteries.

Yong Zhang received his B.S. and M.S. from Xiamen University and Ph.D. from Dartmouth College all in Physics. He joined National Renewable Energy Laboratory (NREL) in 1994 as a postdoc and was a Senior Scientist before he moved to The University of North Carolina at Charlotte as Bissell Distinguished Professor with Electrical and Computer Engineering Department in 2009. His research interests include electronic and optical properties of semiconductors and related nanostructures, organic-inorganic hybrid materials, electronics, and related applications. He has authored more than 250 papers, 5 patents, and edited 3 books. His research works has been cited exceeds 9300 with a H index 47 (in Google Scholar).

Zhong Lin Wang is the Hightower Chair in Materials Science and Engineering and Regents' Professor at Georgia Tech., and the chief scientist and director of the Beijing Institute of Nanoenergy and Nanosystems, Chinese Academy of Sciences. His discovery and breakthroughs in developing nanogenerators and self-powered nanosystems establish the principle and technological road map for harvesting mechanical energy from environmental and biological systems for powering personal electronics and future sensor networks. He coined and pioneered the field of piezotronics and piezophototronics.

Peizhi Yang is a researcher and the director of the Key Laboratory of Advanced Technique & Preparation for Renewable Energy Materials, Ministry of Education at Yunnan Normal University. A science and technology leader in the "Spring City Plan", a Yun Ling Scholar supported by the "Xingdian Yunnan Talent Support Plan", the leader of an innovative team in Yunnan Province, and a spring city industrial mentor; and an expert committee member of the Solar Energy Materials Expert Committee of the China Materials Research Society. He has been engaged in the research of low-dimensional materials and their applications in energy fields, and the development of solar energy efficient material and devices.